Featured in Physics

Excess Noise and Photoinduced Effects in Highly Reflective Crystalline Mirror Coatings

Jialiang Yu,* Sebastian Häfner, Thomas Legero, Sofia Herbers, Daniele Nicolodi, Chun Yu Ma, Fritz Riehle, and Uwe Sterr‡

Physikalisch-Technische Bundesanstalt, Bundesallee 100, 38116 Braunschweig, Germany

Dhruv Kedar, John M. Robinson, Eric Oelker,† and Jun Ye§

JILA, Department of Physics, National Institute of Standards and Technology and University of Colorado, 440 UCB, Boulder, Colorado 80309, USA

(Received 27 January 2023; accepted 7 August 2023; published 3 October 2023)

Thermodynamically induced length fluctuations of high-reflectivity mirror coatings put a fundamental limit on sensitivity and stability of precision optical interferometers like gravitational-wave detectors and ultrastable lasers. The main contribution—Brownian thermal noise—is related to the mechanical loss of the coating material. $Al_{0.92}Ga_{0.08}As/GaAs$ crystalline mirror coatings are expected to reduce this limit. The first measurements of cryogenic silicon cavities revealed the existence of additional noise contributions exceeding the expected Brownian thermal noise. We describe a novel, nonthermal, photoinduced effect in birefringence that is most likely related to the recently discovered birefringence noise. Our studies of the dynamics and power dependence are an important step toward uncovering the underlying mechanisms. Averaging the anticorrelated birefringent noise results in a residual noise that is shown to be substantially different from Brownian thermal noise. To this end, we develop a new method for analyzing the coating noise in higher-order transverse-cavity modes, which makes it possible for the first time to determine the contribution of Brownian thermal noise to the total cavity noise. The new noise contributions must be considered carefully in precision interferometry experiments using similar coatings based on semiconductor materials.

DOI: 10.1103/PhysRevX.13.041002

Subject Areas: Optics, Photonics, Semiconductor Physics

I. INTRODUCTION

Optical interferometers are by far the most sensitive measuring devices: ranging from km-size gravitational-wave detectors [1–4] to cm-size ultrastable resonators [5–9] for the best atomic clocks. For all of these applications, highly reflective mirror coatings are essential. The fundamental displacement noise of the mirror surface, which leads to length fluctuations, must be minimized to reach the ultimate performance. In the most sensitive frequency band of current gravitational-wave detectors, coating noise is one of the main limitations on the strain sensitivity [4]. Optical coatings with lower noise level are indispensable for the tenfold enhanced sensitivity that the next-generation gravitational-wave detectors like the Einstein telescope [4] are aiming for. Noise in optical coatings limits the linewidth of today's most frequency-stable lasers to a few mHz at 1.5 μm. These lasers work as local oscillators for the most precise atomic clocks based on narrow-linewidth optical transitions. Therefore, employing low-noise optical coatings in ultrastable lasers helps to exploit the potential of the microhertz or even nanohertz linewidth of atomic transitions [9–11], which improves the clock stability for investigation of fundamental physics [12–15] and for a future redefinition of the SI second [16,17]. Hence, a considerable number of studies have been carried out over the last decades to reduce mirror noise with novel coating materials [18–23] and advanced mirror concepts [24,25].

According to the fluctuation-dissipation theorem [26,27], the Brownian thermal noise is related to the mechanical dissipation by internal friction [28,29], and it can thus be reduced by using coating materials with lower mechanical loss. Despite significant efforts devoted to the development of improved optical coatings [18–23] including doping [30]

*jialiang.yu@ptb.de

†Present address: University of Glasgow, Institute for Gravitational Research, School of Physics and Astronomy, Glasgow G12 8QQ, United Kingdom.

‡uwe.sterr@ptb.de

§Ye@jila.colorado.edu

and annealing [31], the mechanical-loss coefficients ϕ of characterized conventional dielectric coatings so far have not been improved substantially [32].

A promising approach for further reduction of Brownian thermal noise is provided by crystalline mirror coatings comprised of $Al_{0.92}Ga_{0.08}As/GaAs$ multilayers. These monocrystalline multilayers exhibit lower mechanical loss inferred from mechanical ringdown [33,34] than conventional dielectric coatings ($\phi \approx 4 \times 10^{-4}$ [23,35]). In addition, the optical loss of these coatings has reached a comparable level to that of the dielectric coatings (< 10 ppm), making them an attractive alternative to conventional dielectric coatings. Crystalline coatings were expected to significantly improve the performance of ultrastable lasers and gravitational-wave detectors [3,36]. So far, only a limited amount of experimental data of their coating noise in optical interferometers [37] is available. At room temperature, an ultrastable optical resonator with these coatings has demonstrated lower noise than expected for a similar resonator with dielectric coatings [37]. However, the large noise contribution from other cavity constituents (80%) hindered accurate evaluation of the coating performance, determining the mechanical loss to $\phi = (4 \pm 4) \times 10^{-5}$.

Studying the frequency stability of cryogenic silicon cavities employing these coatings, we have recently discovered novel noise contributions exceeding the expected Brownian thermal noise [38]. While that paper has mostly concentrated on the dependence of the noise on laser power, here, to gain more insight, we first investigate the photo-induced change in the birefringence and its possible contribution to noise. We find a novel nonthermal photo-birefringent effect, which is highly nonlinear in power and which shows a dynamic response with power-dependent timescales of up to several hours. Consequently, we stabilize the power well enough, that the corresponding noise is negligible compared to the newly discovered noise sources.

Second, we investigate the spatial correlation of these noise sources by simultaneously probing different transverse-cavity modes, thereby accessing coating noise independent of technical noise contribution. To this end, we develop a technique where two lasers from opposite sides of the cryogenic cavity are locked to different spatial and polarization eigenmodes of the cavity.

Finally, analyzing the difference between the two Hermite-Gaussian (HG) modes obtained by this method enables us for the first time to directly measure thermal noise of an $Al_{0.92}Ga_{0.08}As/GaAs$ coating at 124 K, and to demonstrate that the previously observed excess noise [38] is not simply Brownian noise from unexpectedly large mechanical loss.

The measurements of the birefringent effects reported in this paper provide a critical lead for future investigations of the origin of the novel noise source presented in semiconductor materials.

II. EXPERIMENT

The intrinsic birefringence of these crystalline coatings [37,39] leads to a splitting of resonator polarization eigenmodes. Frequency noise associated with these individual modes needs special consideration. In our measurements, we can separate three uncorrelated contributions to the fluctuations of the optical path length $d(t)$ for the two polarization eigenmodes averaged over the resonator mode area:

$$d_{\mathrm{slow/fast}}(t) = d_{\mathrm{Brown}}(t) \pm d_{\mathrm{birefr}}(t) + d_{\mathrm{global}}(t). \quad (1)$$

It contains spatially uncorrelated Brownian noise d_{Brown}, fluctuations of the coating birefringence d_{birefr} where $\pm$ applies to the fast and slow polarization eigenmodes, and global excess noise d_{global} with a spatial correlation length larger than the beam diameter. As these contributions are temporally uncorrelated, the total power spectral density (PSD) of the optical length fluctuations S_d is obtained as

$$S_d = S_{\mathrm{Brown}} + S_{\mathrm{birefr}} + S_{\mathrm{global}}, \quad (2)$$

which leads to the same S_d for both polarization eigenmodes.

The schematic overview of our experimental setup is illustrated in Fig. 1. Our optical resonators consist of mirrors with $Al_{0.92}Ga_{0.08}As/GaAs$ crystalline coatings attached on a 21-cm-long monocrystalline silicon spacer [7] operated at 124 K, and on a 6-cm-long [40] spacer operated at 4 or 16 K. The first cavity utilizes two mirrors, both of which have a radius of curvature (ROC) of 2 m, resulting in a mode diameter of 964 μm on both mirrors. Additionally, the second cavity employs two concave mirrors, each with an ROC of 1 m, resulting in a smaller mode diameter of 588 μm. Light propagates between the mirrors in vacuum, and any minute optical path length change Δd can be precisely measured via the shift of the cavity resonance frequency $\Delta\nu$:

$$\Delta d = -\frac{\Delta\nu}{\nu} L_{\mathrm{cav}}, \quad (3)$$

where $\nu = 194$ THz is the laser frequency and L_{cav} is the cavity length.

Thanks to the mechanical loss of single-crystal silicon and the low coefficient of thermal expansion at our operating temperatures [23], the fundamental noise contributions from spacer and mirror substrates, including Brownian thermal noise [41] and thermoelastic noise [42], are an order of magnitude below the predicted coating Brownian noise (see Appendix A 4), which makes these silicon resonators ideal platforms for investigating the coating performance. As there are no measurements of the loss at 124 K, for the prediction we assume that the mechanical loss of these coatings at these cryogenic temperatures is nearly the same as at room temperature

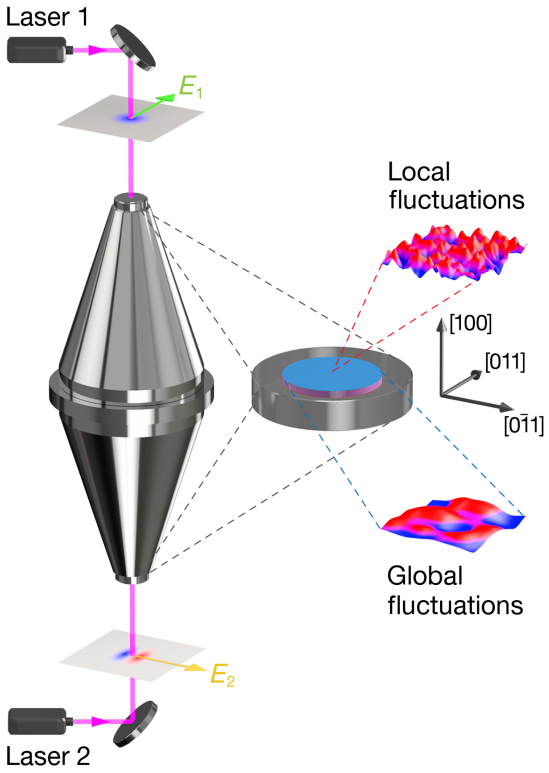

FIG. 1. Schematic of experiment: two lasers are stabilized to the silicon resonator with crystalline mirror coatings. The lasers can be stabilized to different polarization- and transverse-cavity modes independently. Local and global noise sources are depicted in arbitrary units. The frequency fluctuations are measured by comparing the two lasers against a third laser stabilized to a similar reference cavity with dielectric coatings (Si2) [7].

($\phi \approx 2.5 \times 10^{-5}$), even though there is a trend to lower loss at temperatures below 70 K [33].

Static birefringence has been observed in AlGaAs coatings. In our resonators, the [100] crystal direction of GaAs is normal to the mirror surface. We observe that light polarized along the [011] crystal axis (slow axis) exhibits higher refractive index and propagates slower than light polarized along the [0$\bar{1}$1] crystal axis (fast axis), which is consistent with a recent report [39]. For the 6-cm cavity, the mirrors are mounted with parallel orientation $\theta < 3°$ of the GaAs crystal axes, while for the 21-cm cavity, a $\theta \approx 15°$ offset was later discovered. In the 21-cm cavity, this alignment of the coatings splits the resonances into two linearly polarized eigenmodes separated by $\Delta\nu_{\mathrm{birefr}} \approx 200$ kHz, which is much larger than the cavity linewidth of $\Delta\nu_{\mathrm{FWHM}} = 1.8$ kHz. The corresponding static birefringence of the coating multilayer $\Delta n_{\mathrm{birefr}} = n_{\mathrm{slow}} - n_{\mathrm{fast}}$ can be estimated as

$$\Delta n_{\mathrm{birefr}} = \frac{\Delta\nu_{\mathrm{birefr}}}{2\nu} \times \frac{L_{\mathrm{cav}}}{l_{\mathrm{pen}}} \times \frac{1}{|\cos\theta|}, \tag{4}$$

where $l_{\mathrm{pen}} = 163$ nm is the penetration depth [43] of the light field in the coatings, the factor 2 accounts for the two mirrors in the resonator, and $|\cos\theta|$ is the correction factor for axis offset [44]. The corresponding static birefringence (690 ± 3 ppm) is similar to the 6-cm cavity (731 ± 3 ppm) and another room-temperature optical resonator with crystalline coatings at 1.5 μm operated in our lab (792 ± 2 ppm) and is slightly smaller than the value reported in Ref. [37] (1000 ppm).

We stabilize erbium-doped fiber lasers (EDFLs) to our cavities. In the 21-cm cavity, two EDFLs are simultaneously locked on cavity resonances from both ends of the optical resonator via the Pound-Drever-Hall (PDH) technique [45]. This enables us to investigate correlations in optical path length fluctuations between different polarization or transverse eigenmodes, which reveals spatiotemporal properties of the coating noise [46]. The 6-cm cavity system is equipped with one laser only [38].

We systematically characterize and minimize all environmental and instrumental influences, typically referred to as "technical noise" (see Appendix A 1). In total, the technical noise contributions are reduced below the predicted Brownian thermal noise floor between 0.75- and 100-mHz Fourier frequency (see Appendix A 2).

III. RESULTS

A. Photo-birefringent effect

In dielectric [47] and crystalline [48] mirror coatings, it was observed that intracavity power fluctuations lead to optical path length fluctuations. To evaluate this effect in crystalline coatings at cryogenic temperature, we measure the frequency change in response to intracavity power. We observe that the response of the optical path length to a step in the power is opposite for the two polarization eigenmodes (Fig. 2). Initially, the frequency quickly rises to a maximum with a time constant of a few hundred seconds, followed by a slower relaxation with a time constant of several hours. The sensitivity and time constant of the transient response strongly depend on the final intracavity power (see Appendix C 3). Because of the opposite sign between the two polarization axes, this photo-birefringent effect can be canceled with orthogonal alignment of the GaAs crystal axes.

The photo-birefringent effect was not observed in previous studies of the photothermal response of these crystalline coatings [48,49]. This is due to the fact that the photothermal effect in that study is more than 40 times stronger than the photo-birefringent effect observed in this work.

The opposite sign of the transient response cannot be explained by a thermal effect from the absorbed laser power, which is the dominating process in dielectric coatings [42,47], because temperature-induced variation of optical path length is largely polarization independent. We thus attribute this observation to a new light-induced change of birefringence in crystalline coatings (photo-birefringent effect). A length change of $\Delta d = 1 \times 10^{-14}$ m in Fig. 2

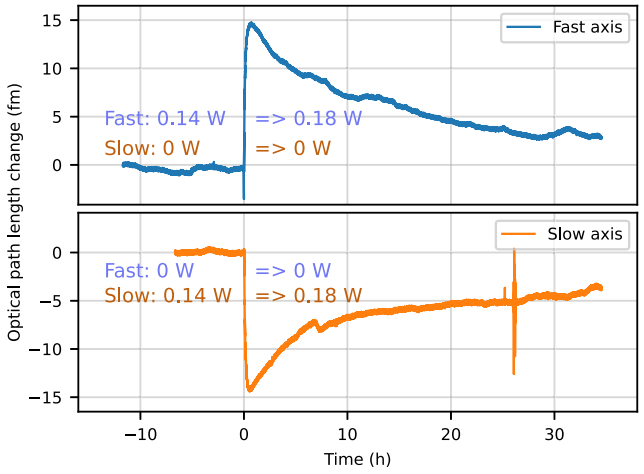

FIG. 2. Single-polarization transient response of the 21-cm cavity to a step change of intracavity power measured in succession. The optical path length changes of the fast (blue) and the slow (orange) axes are symmetric.

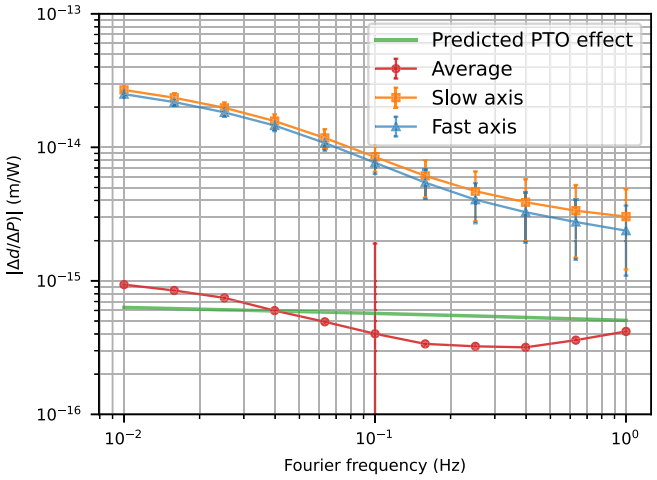

FIG. 3. Frequency dependence of optical path length changes to intracavity power variations for fast (blue) and slow (orange) axes and for their average (red) at mean intracavity power of 0.54 W in comparison to the theoretical photothermal optic response (green) calculated according to Ref. [47]. The error bars indicate the 95% confidence interval. It includes statistical uncertainty and possible contributions due to slowly varying electronic offsets in the measurement. The latter contribution is estimated by forwarding typical electronic offsets to the slope of PDH error signal. For the red curve, only one representative error bar is shown.

corresponds to a change of birefringence $\delta n_{\mathrm{birefr}} = \delta n_{\mathrm{slow}} - \delta n_{\mathrm{fast}} = 3 \times 10^{-8}$ according to Eq. (4) (45 ppm of the static birefringence $\Delta n_{\mathrm{birefr}}$).

Such a behavior is not seen in our otherwise identical reference silicon resonators with dielectric coatings (Si2 and Si4) [7,40]; therefore, this photo-birefringent effect results presumably from the semiconducting properties of the crystalline coatings.

While a full theoretical model has not yet been developed, we speculate that the photo-birefringent effect may be related to the linear electro-optic effect [50], as light-induced birefringence has been observed in other materials [51–53].

For crystalline coatings, the crystal orientation of the photo-birefringent effect can be explained by a change in the electric field of 3 kV/m perpendicular to the coating surface, which is a relatively small magnitude compared to the 100-times-larger electric field strength observed in some heterojunctions [54].

To investigate the power dependence of the photo-birefringent effect, we change the intracavity power of the laser locked on the slow axis in the three steps (0.6 ⇒ 0.2 W, 0.6 ⇒ 1.6 W and 1.6 ⇒ 0.6 W), and no optical power is coupled to the fast axis. The path length change is inferred from the observed change in optical frequency $\Delta\nu$ as $\Delta d = -L_{\mathrm{cav}}\Delta\nu/\nu$. The normalized transient response of the optical path length shown in Fig. 4 indicates a strong dependence of its amplitude and time constant on the final optical power.

To evaluate the influence of laser power noise on the optical path length fluctuations imposed by the photo-birefringent effect, we measure the small-signal transfer function from power to frequency (Fig. 3). The measured transfer functions for two polarization axes are very similar as they are dominated by the photo-birefringent effect. The average of their complex amplitudes is the transfer function of the polarization-averaged response after removing the photo-birefringent effect. This transfer function is compatible with that of the photothermal optical effect [47]. Because of the large uncertainty in the small difference, the remaining frequency dependence is insignificant. For the two polarization eigenmodes, the sensitivity of the optical path length to power fluctuations decreases with increasing intracavity power (see Appendix C 3).

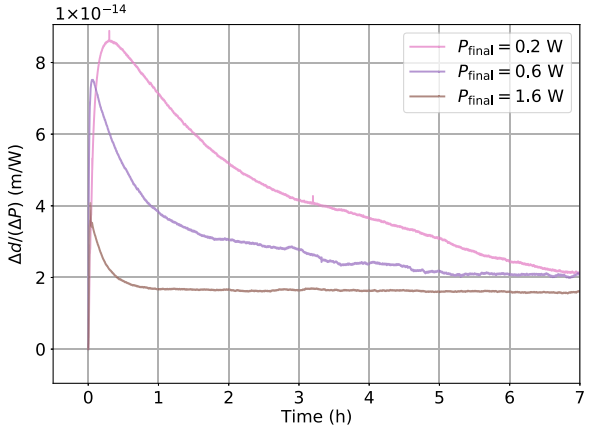

FIG. 4. Normalized response of the optical path length Δd (slow axis) to a step ΔP in intracavity optical power. Both amplitude and time constant show a strong dependence on the final intracavity power P_{final}.

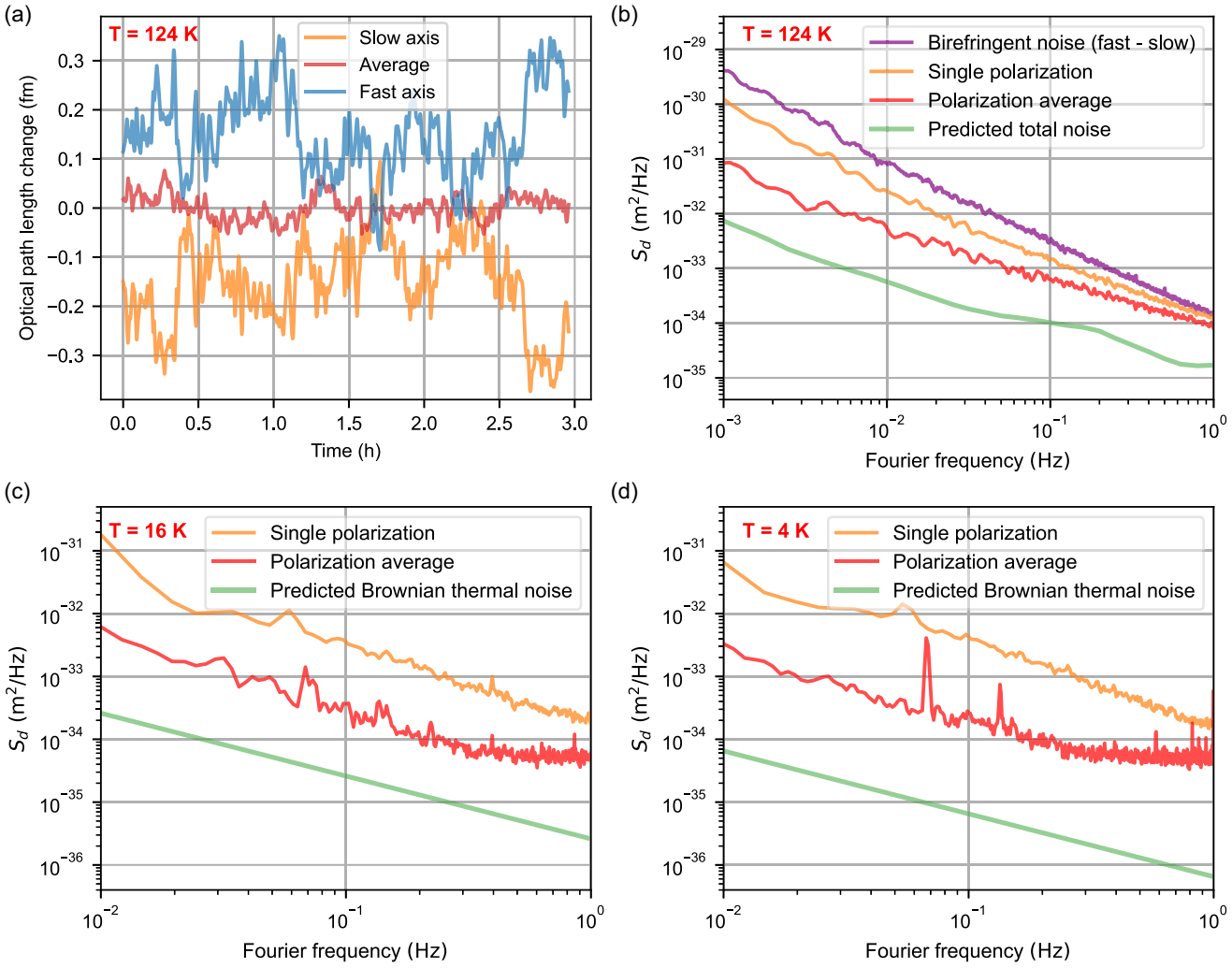

FIG. 5. (a) Optical path length fluctuations of the 21-cm cavity measured with the beat signal between Si2 and the two polarization eigenmodes with intracavity power of 1.3 W in the fast and 0.7 W in the slow axis (blue, orange). The noise from Si2 is below the average of the two polarization eigenmodes (red). (b) Power spectral densities S_d of the length fluctuations in the 21-cm cavity. Birefringent noise (purple), noise of an individual polarization eigenmode (orange), and average of two polarizations (red). The sum of technical noise contribution and the predicted Brownian thermal noise for the Hermite-Gaussian HG_{00} mode (green) is included for comparison. (c),(d) Power spectral densities S_d of the length fluctuations in the 6-cm cavity at 16 (c) and 4 K (d). Frequency stability of individual polarization eigenmodes (orange) of the average of two polarization eigenmodes (red) and the predicted Brownian thermal noise (green). The contribution of reference lasers is removed from the PSDs (see Appendix A).

The decrease in the transfer function toward high frequencies corresponds to the fast initial step response (Fig. 2). The long-term behavior is not visible in the single-polarization transfer functions due to limitations of the lowest measurable frequencies.

From these transfer functions, we conclude that with our actively stabilized optical power, the optical path length noise related to the photo-birefringent effect of $S_d = 2 \times 10^{-36}\,\mathrm{m}^2/\mathrm{Hz} \times (f/\mathrm{Hz})^{-1}$ is suppressed well below the predicted coating Brownian thermal noise (see Appendix A 2).

B. Birefringent noise

With all relevant technical noise sources suppressed below the expected Brownian thermal noise, we lock the two independent lasers to the fundamental HG mode of the 21-cm cavity with different polarizations. The mirror coating noise is observed as the frequency fluctuations of the two lasers compared to the Si2 reference laser [Fig. 5(a)].

We observe strongly anticorrelated frequency fluctuations between the two polarization eigenmodes. Observing the frequency difference of the two lasers suppresses all common mode noise contributions leaving only the birefringence fluctuations [purple curve in Fig. 5(b)].

These so far unobserved intrinsic birefringence fluctuations ("birefringent noise") in crystalline coatings lead to optical path length fluctuations with PSD two orders of magnitude higher than the predicted Brownian thermal

noise [Fig. 5(b)]. The same behavior is observed in the 6-cm cavity at 16 and 4 K [Figs. 5(c) and 5(d)]. In Figs. 5(b)–5(d), the impact of polarization averaging gradually diminishes at higher Fourier frequencies as other noise contributions come into play. For the 124-K measurement, a common mode noise (see Sec. II C) becomes a significant contribution to the total coating noise, while in Figs. 5(c) and 5(d), the limit originates from a technical noise as discussed in Ref. [38]. We also find that the birefringent noise slightly increases with optical power [38].

Unlike photo-birefringent noise, the birefringent noise will not be suppressed by orthogonal alignment of the GaAs crystal axes, because the birefringence fluctuations of individual crystalline coatings are uncorrelated.

C. Polarization-independent noise contributions

By simultaneously probing the two polarization eigenmodes with two independent lasers, we are able to remove the anticorrelated birefringent noise by polarization averaging. Nevertheless, we observe at all three temperatures a remaining noise level that is still significantly higher than the predicted coating Brownian thermal noise. This remaining noise is independent of optical power, which indicates a noise mechanism different from the birefringent noise described in the previous section. The remaining noise roughly has a $1/f$ dependence in PSD akin to Brownian thermal noise (Fig. 5, red lines). This noise level could be, in principle, explained by an increased coating mechanical loss ϕ. While there are reliable data for the mechanical loss from cantilever ringdown measurement at high frequencies at 4, 16, and 300 K, no direct loss measurements of coatings at low frequencies and at 124 K are available. To measure the relevant loss $\phi_{124\,\mathrm{K}}$, we analyze the spatial correlations of the polarization-independent remaining noise.

For dielectric coatings, Brownian thermal noise is the leading spatial uncorrelated noise source (local noise) with a correlation length on the order of coating thickness, and thus, it shows up in the difference in displacement fluctuations between two different HG modes. Global noise sources with correlation length much larger than the mode diameter of 1 mm are common to both modes and are strongly suppressed in this difference [55].

The technical difficulty associated with this method in crystalline coatings is that the birefringent noise is also local noise (see Appendix C 2): To investigate the spatial correlation of the polarization-averaged remaining noise between the HG_{00} and HG_{01} modes, four lasers are required to average the two polarization eigenmodes of both HG modes, respectively, resulting in considerable additional complexity.

To solve this problem, we develop a dual-frequency locking technique that enables the cancellation of birefringent noise using only one laser for each HG mode. This is achieved by simultaneous excitation of both polarization eigenmodes using additional spectral lines generated with an electro-optic modulator. In this way, an overall error signal containing equally weighted contributions from both polarization eigenmodes is generated; thus, the laser can be stabilized to their average. With this dual-frequency locking technique, we suppress the birefringence noise by more than two orders of magnitude, and the locking noise is well below the predicted coating Brownian thermal noise. More details about this technique can be found in Appendix B.

We stabilize one laser coupled from the top of the cavity to the polarization-averaged HG_{00} mode. The other laser is stabilized simultaneously to the averaged HG_{01} mode from the bottom of the cavity. Even though there is a certain overlap of these two modes, they probe fluctuations averaged over significantly different areas of the mirror coatings. The displacement fluctuations are measured by referencing the two laser frequencies to the Si2 system [Fig. 6(a) blue and orange]. These measured fluctuations contain (similar) contributions from the cavity with crystalline coatings and from the Si2 reference cavity (see Appendix C 1).

The fluctuations visible in the direct difference between the two HG modes [Fig. 6(a) red] contain only local noise such as Brownian thermal noise, but no correlated global noise [Eq. (1)]. Thus, this difference constitutes an upper bound on the coating Brownian thermal noise. Figure 6(b) compares the power spectral densities $S_d^{(\Delta)}$ of the measured fluctuations against that predicted from coating Brownian thermal noise. The measured displacement noise in the difference of the two modes [Fig. 6(b) red] corresponds to a loss coefficient $\phi_{300\,\mathrm{K}} \approx 2.5 \times 10^{-5}$. Loss coefficients from ringdown measurements are available only near room temperature ($\phi_{300\,\mathrm{K}} \approx 2.5 \times 10^{-5}$ [37], $\phi_{300\,\mathrm{K}} \approx 4.78(5) \times 10^{-5}$ [34]) and below 70 K [33] with a trend toward lower loss at low temperatures. Thus, the mechanical loss relevant for precision interferometry at 124 K shows no unexpected behavior to the value obtained from mechanical ringdown at different frequencies and temperatures.

With this precisely determined local noise $S_d^{(\Delta)}$, we can calculate its contribution to the individual displacement fluctuations averaged over the HG_{00} and HG_{01} modes. The corresponding PSDs are $S_{\mathrm{local}}^{(00)} = 1.33 \times S_d^{(\Delta)}$ for the HG_{00} mode and $S_{\mathrm{local}}^{(01)} = 1.00 \times S_d^{(\Delta)}$ for the HG_{01} mode (see Appendix C 1). The PSD in Fig. 6(b) obtained from the three-cornered-hat method, where the contribution from Si2 is removed, clearly shows that the observed noise in the individual modes is one order of magnitude larger than the value calculated from these numbers ($1.33 \times S_d^{(\Delta)}$). Therefore, the displacement noise experienced by the modes is dominated by a nonlocal noise process with spatial correlation lengths larger than the mode size. This global excess noise d_{global} also appears to be a persistent source of noise at 4 and 16 K, as recorded also for the 6-cm cavity [Figs. 5(b) and 5(c)] [38].

In principle, technical noise or hitherto unobserved noise, e.g., from optical contacts, could appear as such a

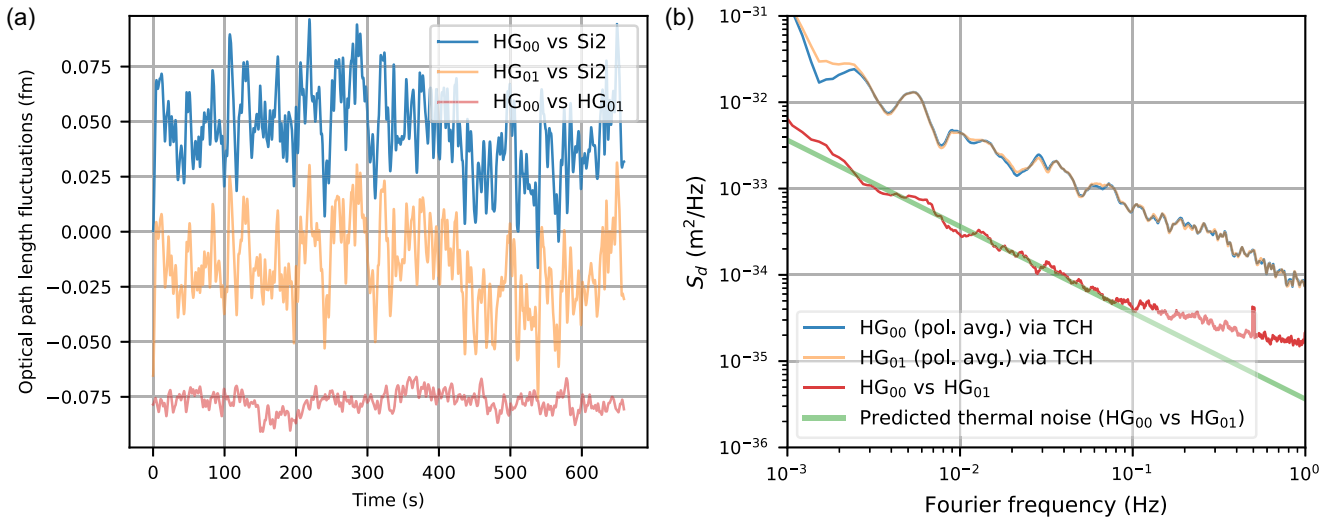

FIG. 6. (a) Measured optical path length fluctuations of polarization-averaged the HG_{00} (blue) and HG_{01} modes (orange) referenced to another cavity (Si2), and the difference between the two HG modes (red). For clarity, the curves are shifted by an arbitrary amount. (b) Spectral power densities of the individual displacement noise of the HG_{00} (blue) and HG_{01} modes (orange) determined by three-cornered-hat (TCH) method, and of their difference (red). The estimated differential Brownian noise between the two modes is shown in green.

global noise. However, all known technical noise contributions are found to be significantly lower than the observed global noise (see Appendix A 2). Moreover, the detection of this novel global noise in two independent systems in separate laboratories makes underestimated technical noise unlikely. Additionally, the close agreement between the experimentally observed noise in all our cavities using conventional coatings [7,40] and the theoretically expected noise based on loss measurements of these dielectric coatings leaves little room for additional noise sources of comparable magnitude.

In summary, these facts make us confident that this novel global excess noise is most likely intrinsic to the crystalline coating.

IV. CONCLUSION AND DISCUSSION

We investigate the properties related to the recently discovered noise in AlGaAs crystalline mirror coatings [38] under conditions relevant for precision interferometry with two different cryogenic silicon cavities at 4, 16, and 124 K.

We discover a nonthermal photo-birefringent effect, which is a change in the static coating birefringence depending on laser power at the mirror. We show that with sufficiently stabilized laser power its contribution to the interferometer noise is negligible, and thus, this effect cannot explain the recently discovered noise in AlGaAs coatings.

We can distinguish three fundamental contributions to the novel noise. The biggest contribution is birefringent noise. We present and evaluate a technique to cancel this noise by averaging both polarization eigenmodes.

We investigate the $1/f$ global excess noise that remains after canceling birefringent noise. It is characterized by comparing different spatial modes, and we show that it is not related to technical noise. Most likely, it is associated with the semiconductor properties of the coatings.

With this method, we unambiguously show that the coating Brownian noise at 124 K is in very good agreement with the theoretical prediction obtained from the room-temperature mechanical-loss factor, thus confirming the expected Brownian noise reduction in AlGaAs crystalline coatings.

The first two contributions are significantly higher than the Brownian thermal noise which has significant implications for the use of current crystalline coatings in future ultrasensitive interferometers.

In our ultrastable lasers based on cryogenic silicon cavities, crystalline coatings suffer from birefringent noise and therefore exhibit significantly inferior performance than dielectric coatings. After suppressing the birefringent noise by polarization-averaging, the PSD of crystalline coatings is reduced compared to conventional dielectric coatings, with a ratio of $S_d^{(\mathrm{crys})}/S_d^{(\mathrm{dielec})} = 0.77$ at 4 K, 0.38 at 16 K, and 0.83 at 124 K. The superiority at 16 K stems from two factors: (1) The global excess noise does not show strong temperature dependence, while thermal noise increases linearly with the temperature. (2) The smaller mode area in the 6-cm cavity would lead to pronounced Brownian thermal noise if dielectric coatings are utilized. For cavities operating at room temperature or other wavelengths, further investigations are still required.

Third-generation cryogenic gravitational-wave detectors such as the low-frequency Einstein Telescope (ET LF) [4]

are proposed to operate at a quite similar temperature, wavelength, and intracavity laser intensity as the 6-cm cavity, except the 300-times-larger beam radius. Extrapolating our results, we conclude that the current crystalline coatings would lead to higher noise than the dielectric coatings in these systems (see Appendix D), even if the birefringent noise could be canceled and the correlation length of the global excess noise would be only on the order of 1 mm—the lower limit deduced from our measurement—which would allow us to spatially average the excess noise. Similarly, by extrapolating our results from our 21-cm resonator, we estimate the potential performance of crystalline coatings in the LIGO Voyager [3]. Our findings indicate that current crystalline coatings would result in approximately 90% higher noise PSD than conventional dielectric coatings. Therefore, current crystalline coatings have no advantage over the conventional dielectric coatings in third-generation cryogenic gravitational-wave detectors.

As the mechanisms for the two new noise processes might be related to defects and impurities [56,57] of the semiconductor coating, a better understanding of the microscopic effects could lead to a reduction of the noise. This knowledge will also be helpful to other semiconductor-based coatings, such as aSi/SiN [58], that are currently discussed for precision interferometry. Our findings indicate that a broader investigation of noise processes in a wider class of semiconductor materials is important, which might shed further light on the underlying mechanisms.

ACKNOWLEDGMENTS

We acknowledge support by the Project 20FUN08 NEXTLASERS, which has received funding from the EMPIR programme cofinanced by the Participating States and from the European Union's Horizon 2020 Research and Innovation Programme, and by the Deutsche Forschungsgemeinschaft (DFG, German Research Foundation) under Germany's Excellence Strategy–EXC-2123 QuantumFrontiers, Project-IDs No. 390837967, No. SFB 1227 DQ-mat, and No. 274200144. This work is partially supported by the Max Planck-RIKEN-PTB Center for Time, Constants and Fundamental Symmetries. This work is also supported by NIST, DARPA, AFRL, and JILA Physics Frontier Center (NSF Grant No. PHY-1734006).

APPENDIX A: EXPERIMENTAL SETUPS

1. Cryogenic silicon resonators

The 21-cm silicon resonator (Si5) in this experiment is set up and operated at PTB, Germany to investigate the noise from crystalline mirror coatings. The mirror pair reaches finesse values of $(3.65 \pm 0.01) \times 10^5$ for the fast axis and $(3.58 \pm 0.01) \times 10^5$ for the slow axis, corresponding to a total loss of 17.4 and 17.8 ppm, respectively. The Si5 setup is based on our previous design of silicon resonators that are equipped with dielectric coatings (Si2 and Si3). The temperature of Si5 is also controlled with cold nitrogen gas [59]. Si2 and Si3 demonstrate the Brownian thermal noise limited performance of $S_d = 8 \times 10^{-35}/(f/\mathrm{Hz})\ \mathrm{m}^2/\mathrm{Hz}$ between 0.01 and 10 Hz Fourier frequency after suppression of technical noise [7] (Si3 is later transferred to our lab in JILA).

Compared to previous systems, we further suppress technical noise in Si5: Residual amplitude modulation (RAM) is suppressed in both laser systems from both ends [60]. Optical path length fluctuations in the setup (fiber and free space) are actively canceled [61] in addition to a free-space path of less than 30 cm. This ensures much lower fiber noise level compared to the predicted Brownian thermal noise. Frequency fluctuations of the two lasers are measured by referencing them to Si2 [7]. Frequency fluctuations between the two lasers are detected directly by a photodetector, where the transmitted light of the far-end laser and the reflected sidebands of the near-end laser interfere, thus avoiding any uncompensated optical path. We actively suppress the seismic noise with a commercial antivibration platform, and improve it for Fourier frequencies above 0.1 Hz with an additional low-frequency feedback loop including high-performance seismometer and tiltsensor [62]. Parasitic etalons are identified by correlating ambient pressure with frequency fluctuation of the resonator at Fourier frequencies below 10 mHz, and are reduced by tilting optical surfaces and adding optical isolators. With technical noise suppressed, Si5 facilitates the investigation of the Brownian thermal noise from the two crystalline coatings of $S_d = 1 \times 10^{-36}/(f/\mathrm{Hz})\ \mathrm{m}^2/\mathrm{Hz}$ (see Appendix A 2).

To determine the PSDs of frequency noise from Si5 in Figs. 5(b) and 6(b), we apply the three-cornered-hat analysis [63] to the PSD. This method requires two additional independent reference resonators, involving Si2 and a second reference laser at 698 nm stabilized to a 48-cm room-temperature cavity with dielectric coatings attached on a spacer made of ultralow-expansion (ULE) glass [6], and the frequency gap is bridged by an optical frequency comb. We measure beat notes between these systems (Si5-Si2, Si5-ULE, and Si2-ULE) with lambda-type zero-dead-time frequency counters, and calculate the PSDs of their frequency fluctuations. Assuming uncorrelated noise in the three systems, the noise PSD of Si5 can be obtained as

$$S_d^{(\mathrm{Si5})} = \frac{1}{2}\left(S_d^{(\mathrm{Si5-Si2})} + S_d^{(\mathrm{Si5-ULE})} - S_d^{(\mathrm{Si2-ULE})}\right). \quad \text{(A1)}$$

The 6-cm resonator with crystalline coatings (Si6) is located in JILA, USA. This system is based on the design of Si4 [40], which is cooled with a closed-cycle cryostat, and its temperature can be varied between 4 and 16 K. The performance of Si6 is determined by subtracting the noise of Si3, which is carefully characterized with a strontium lattice clock in the same lab [9], from the beat with Si3.

TABLE I. Key differences among cryogenic silicon cavities.

Name	Si1/2/3	Si4	Si5	Si6
Cavity length (m)	0.21	0.06	0.21	0.06
Temperature (K)	124	4/16	124	4/16
Optical coating	Dielectric	Dielectric	Crystalline	Crystalline

Detailed characterization of various technical noise is reported in Ref. [38]. Briefly, the 6-cm cavity has a birefringent mode splitting of 770 kHz. An interrogation scheme different from Si5 is employed, where both polarization modes are simultaneously probed with phase modulation sidebands of a single laser to cancel the birefringent noise. The residual noise is found to be of similar scale to that of Si5. Comparison between Si5 (124 K) and Si6 (4.7 and 16.7 K) thus offers a unifying view of the residual global noise. Si6 realizes a frequency stability of mod $\sigma_y = 5.5 \times 10^{-17}$ with excellent long-term performance.

A brief summary of the cryogenic silicon resonators is given in Table I.

2. Thermal noise budget of the 124-K system

The thermal noise budget for the power spectral density of length fluctuations $S_d(f)$ in the 21-cm resonator (Si5) with AlGaAs mirror coatings is illustrated in Fig. 7. The Brownian thermal noise of the cavity constituents is calculated with the equations from Ref. [41], while the material properties are taken from Refs. [37,59]. Thermo-optic noise is calculated by averaging the thermal expansion and refractive index change, which are induced by the thermal fluctuations, across the mode area [64]. The Brownian thermal noise contributions from the AlGaAs coating is by far the biggest contribution for all considered frequencies.

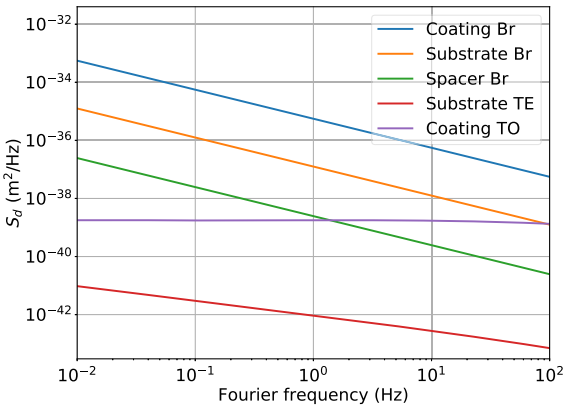

FIG. 7. Thermal noise contributions in the Si5 resonator. Br, Brownian thermal noise; TE, thermoelastic noise; TO, thermo-optic noise.

3. Resonator parameters

The resonator parameters used for the calculation of thermal noise and photo-optic response are summarized in the following tables: Table II for the properties of the optical resonators and Table III for the coating parameters.

4. Technical noise budget of the 124-K system

The main technical noise contributions are carefully characterized and minimized as described in Appendix A 1. The result of the 21-cm silicon resonator is shown in Fig. 8. It includes the contribution from vibrations calculated from the measured sensitivities and the vibrations at the cavity, parasitic etalons that are investigated from the observed frequency shifts induced by ambient pressure. The influence of the temperature is estimated from observed temperature fluctuations, including the thermal model and the estimated thermal expansion coefficient of the cavity. The pressure influence is based on the measured pressure fluctuations and the refractivity of air [74]. Light dissemination noise results from optical path length fluctuations in unstabilized free space and short fiber sections. The contribution from photo-birefringence is based on the measured sensitivities (see main text) and measured intracavity power fluctuations. Influence of RAM and electronics is based on independently measured error signals.

TABLE II. Parameters for optical resonators.

Parameter	Value
21-cm cavity	
Cavity length	0.212 m
Spacer radius	0.04 m
Radius of central bore	5 mm
ROC of mirror	2 m
Beam radius on mirror	482 μm
Cavity temperature	124 K
Cavity finesse	3.6×10^5
Laser wavelength	1542 nm
6-cm cavity	
Cavity length	0.06 m
ROC of mirror	1 m
Beam radius on mirror	294 μm
Cavity temperature	4 or 16 K
Cavity finesse	2.9×10^5
Laser wavelength	1542 nm
Single-crystal silicon	
Young's modulus	188 GPa [65]
Poisson ratio	0.26 [65]
Density	2331 kg/m^3 [66]
Thermal conductivity	600 W/m K [67]
Specific heat	330 J/kg K [68]
Mechanical loss	0.83×10^{-8} [69]

TABLE III. Parameters for the crystalline coating.

Parameter	Value
Optical coating	
Coating structure	$\mathrm{GaAs} + 45(\mathrm{AlGaAs} + \mathrm{GaAs})$
Layer optical length	Quarter wavelength
Coating total thickness	11.68 μm
Coating mechanical loss	2.5×10^{-5} [34,37]
$Al_{0.92}Ga_{0.08}As$	
Layer thickness	132.634 nm
Young's modulus	83 GPa [70]
Poisson ratio	0.40 [70]
Density	3885 $\mathrm{kg/m^3}$ [70]
Refractive index	2.9065 [71]
Temperature coefficient of n	0.99×10^{-4}/K [71]
Thermal conductivity	69 W/m K [72]
CTE (GaAs)	3×10^{-6}/K
Specific heat	313 J/kg K
GaAs	
Layer thickness	115.477 nm
Young's modulus	86 GPa [70]
Poisson ratio	0.31 [70]
Density	5317 $\mathrm{kg/m^3}$ [70]
Refractive index	3.3383 [73]
Temperature coefficient of n	1.75×10^{-4}/K [73]
Thermal conductivity	100 W/m K [73]
CTE	3×10^{-6}/K [70]
Specific heat	215 J/kg K [73]

In the range between 0.75 and 100 mHz, technical noise contributions are mostly below the predicted Brownian thermal noise.

Thermal noise from the bonding of the crystalline coatings to the silicon mirror substrate should have similar spatial property (local) as the optical coating noise, as this bonding can be approximately treated as an additional layer on the coating with different mechanical loss. Therefore, the long spatial coherence length of the excess noise cannot be explained by this source.

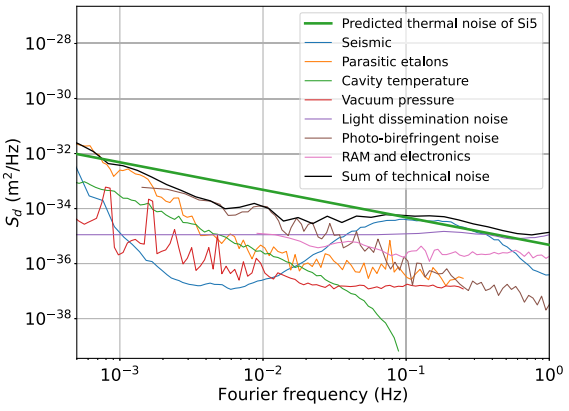

FIG. 8. Technical noise contributions for Si5 in comparison to the Brownian noise of the AlGaAs/GaAs coating with $\phi_{124\,\mathrm{K}} = 2.5 \times 10^{-5}$.

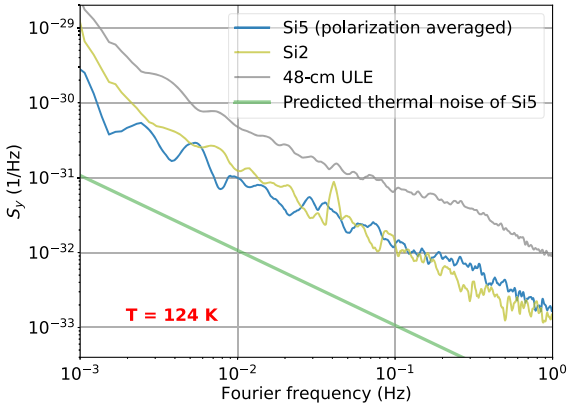

FIG. 9. Obtained by the three-cornered-hat analysis: PSD of fractional frequency noise of Si5 (blue), Si2 (yellow), and the 48-cm ULE cavity (gray). The expected thermal noise of Si5 (green) is included for reference.

Brownian noise from the silicon spacer or the mounting would appear as global noise. This would require an increase of the loss coefficient of silicon by more than an order of magnitude compared to well-established values. In addition, there is also no visible difference of the excess noise level between 4 and 16 K which would appear in this case, as the loss coefficient is constant in this range [69].

5. Instability of the 124-K setup from three-cornered-hat analysis

The performance of the 21-cm resonator is determined by analyzing the beat signals with two additional oscillators as explained in Appendix A 1. The result of this analysis is the power spectral density of fractional frequency fluctuations $S_y(f)$, which is displayed in Fig. 9. The corresponding spectrum of fluctuations d of the total optical length L_{cav} between the mirrors is calculated as $S_d = L_{\mathrm{cav}}^2 S_y$.

The stability of Si5 outperforms Si2 at lower Fourier frequencies, because Si2 suffers from strong parasitic etalons. Owing to better suppression of parasitic etalons, Si5 has a much better long-term stability than the other two systems. The performance of the reference system for characterization of Si6 is described in Ref. [9].

APPENDIX B: AVERAGING BIREFRINGENT NOISE: DUAL-FREQUENCY LOCK

In this section, we describe the simple dual-frequency locking scheme that is used in our experiment to cancel the anticorrelated birefringent noise. Using a single laser beam from one side of the cavity, this method generates an error signal with equal contributions from both polarization eigenmodes. This technique is much simpler than using two separate lasers from both ends, which requires two

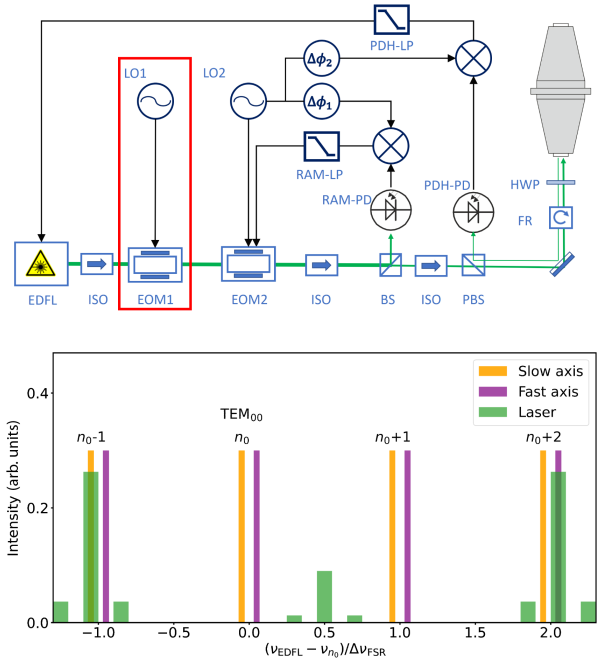

FIG. 10. Top: experimental setup of the locking scheme. The additional EOM1 and its driver LO1 required for dual-frequency locking are shown in the red box. EDFL, erbium-doped fiber laser; ISO, optical isolator; EOM, electro-optic modulator; (P)BS, (polarization) beam splitter; FR, Faraday rotator; HWP, half wave plate; PD, photodetector; LP, loop filter; LO, local oscillator. Bottom: frequency components of the light (green), and the cavity resonances of fast (purple) and slow (red) axes in units of the free spectral range $\Delta\nu_{\mathrm{FSR}}$.

independent locking setups including separate RAM control, laser power stabilization, and fiber noise cancellation. The main building blocks of this locking scheme are shown in Fig. 10. The scheme is largely based on the usual PDH setup [75] with RAM compensation [76] and only an additional EOM to generate sidebands (red box in Fig. 10) is required.

In dual-frequency locking, the in-coupling light at the front mirror is linearly polarized at 45° relative to both axes (fast and slow). The first-order sidebands of an electro-optic modulator (EOM1 in Fig. 10) are used to excite the two polarization eigenmodes and generate a PDH error signal given by the sum of both modes. The modulation index of EOM1 is set to $M = 1.8$ rad to maximize the optical power in the two sidebands. Scanning the laser frequency over the cavity resonance, the PDH signal shows three components: when the upper sideband is resonant with the slow axis ($\nu_{\mathrm{slow}} < \nu_{\mathrm{fast}}$), when both sidebands are in resonance with their corresponding polarization eigenmodes, and when the lower sideband is resonant with the fast axis. By locking to the central error signal, the laser is stabilized to the average of two polarization eigenmodes if the error signals from both modes are equally weighted. The RAM control loop stabilizes in this case the RAM of the sum of all the spectral lines generated by EOM1, which is dominated by the first-order sidebands used for dual-frequency locking. Stabilizing the laser using first-order sidebands on the two polarization eigenmodes of the same longitudinal mode ($f_{\mathrm{mod1}} = 0.5\Delta\nu_{\mathrm{birefr}}$) is not advisable. The small separation between the spectral lines would lead to significant coupling of noise in the wings of one sideband to the adjacent polarization eigenmode, and the undesired interference with the other sideband would degrade the frequency stability. Thus, the modulation frequency f_{mod1} of EOM1 is set to address polarization modes separated by at least one free spectral range $\Delta\nu_{\mathrm{FSR}}$:

$$f_{\mathrm{mod\,1}} = (n + 0.5)\Delta\nu_{\mathrm{FSR}} \pm 0.5\Delta\nu_{\mathrm{birefr}}, \quad n = 0, 1, 2\ldots \tag{B1}$$

If only one laser is stabilized to the resonator via dual-frequency locking, n can be set to 0 ($f_{\mathrm{mod1}} \approx 0.5\Delta\nu_{\mathrm{FSR}}$). To lock two lasers simultaneously with dual-frequency locking from opposite sides of the resonator, we choose $f_{\mathrm{mod1}} = 1.5\Delta\nu_{\mathrm{FSR}} + 0.5\Delta\nu_{\mathrm{birefr}}$ to avoid crosstalk between the two lasers and to simplify the beat detection for frequency counting: The smallest beat frequency between the top and bottom lasers is obtained by locking the two lasers to adjacent cavity modes and by generating a beat between one of the first-order sidebands of the bottom laser (transmission) and the off-resonance carrier of the top laser (reflection).

The performance of the dual-frequency lock is reduced by the smaller error signal in comparison to normal PDH locking and the imperfect weighting of the error signals of the two polarizations. The smaller error signal arises from the polarization mismatch between the incident light field and the polarization axes of the resonator, as only half of the optical power of the corresponding spectral lines can be coupled into the cavity and contributes to the error signal. To balance the error signals from the two polarization

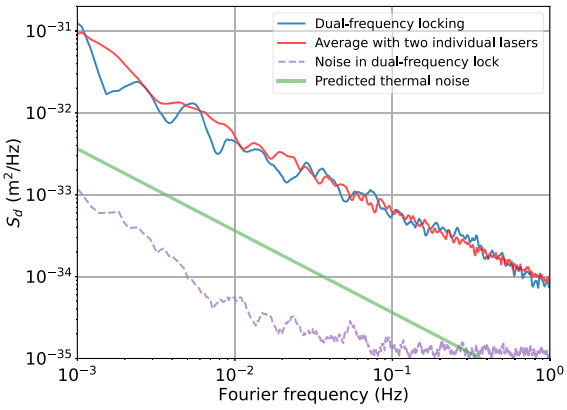

FIG. 11. PSD of dual-frequency locking (blue) compared to that achieved by averaging with two independent laser setups. The PSD of the difference between two lasers stabilized to adjacent HG_{00} modes with dual-frequency locking indicates the quality of this technique. Both methods suppress the birefringent noise by at least a factor of 10.

eigenmodes, we optimize the settings of the half wave plate in front of the resonator. From the comparison with locking two independent lasers and thus perfect averaging (Fig. 11), a similar suppression of birefringent noise is achieved, which corresponds to a tenfold reduction of birefringent noise in PSD [Fig. 5(b)].

To evaluate the ultimate noise of this method, we stabilize both lasers via dual-frequency locking to adjacent polarization-averaged TEM_{00} modes. The noise between the two lasers shows a total noise level well below the global excess noise and even below the predicted coating Brownian thermal noise (see Fig. 11).

APPENDIX C: EXPERIMENTAL METHODS AND FURTHER RESULTS

1. Spatial correlation of Brownian thermal noise

According to the fluctuation-dissipation theorem, the PSD of Brownian thermal noise is proportional to the average dissipated power W_{diss} when a pressure with the shape of the beam intensity profile generated by a force F_0 oscillating at the corresponding frequency f is applied [28,41]. Provided the mode diameter is much larger than the coating thickness, the single-sided PSD of the coating Brownian thermal fluctuations probed by an HG_{mn} mode is

$$S^{(mn)}_{\mathrm{Brown}} = \frac{2k_BT}{\pi^2 f^2} \times \frac{W^{(mn)}_{\mathrm{diss}}}{F_0^2} = g_{(mn)} \times \frac{4k_BT(1+\sigma_{\mathrm{sub}})(1-2\sigma_{\mathrm{sub}})d_{\mathrm{ct}}}{\pi^2 f w^2 E}\phi_{\mathrm{ct}}, \quad \text{(C1)}$$

where k_B is the Boltzmann constant, T is the resonator temperature, σ_{sub} and E are the Poisson ratio and Young's modulus of mirror substrate, f is the Fourier frequency, w is the $1/e^2$ beam radius on the mirror, and d_{ct} and ϕ_{ct} are the thickness and mechanical loss of the coating. The merit factor $g_{(mn)} = S^{(mn)}_{\mathrm{Brown}}/S^{(00)}_{\mathrm{Brown}}$ was introduced by Vinet [77] to describe the scaling of Brownian thermal noise between the HG_{00} and HG_{mn} modes:

$$g_{(mn)} = \frac{4}{\pi}\int_0^\infty dp \int_0^\infty dq e^{-(p^2+q^2)}(L_m(p^2) \times L_n(q^2))^2, \quad \text{(C2)}$$

where $L_m(x)$ is the mth ordinary Laguerre polynomial. Table IV gives the first $g_{(mn)}$ factors, and the factor relevant for this work is $g_{(00)}/g_{(01)} = 1.33$.

TABLE IV. Numerical values for $g_{(mn)}$, the relative PSD of HG_{mn} to HG_{00}.

n \ m	0	1	2	3
0	1.000	0.750	0.641	0.574
1	0.750	0.563	0.480	0.431
2	0.641	0.480	0.410	0.368
3	0.574	0.431	0.368	0.330

The predicted Brownian thermal noise for the 21- and 6-cm silicon resonators at different operating temperatures is shown in the green curves in Figs. 5(b)–5(d). Similarly, the fluctuations of the frequency difference between Hermite-Gaussian modes HG_{mn} and HG_{00} induced by coating Brownian thermal noise $S^{\Delta(mn)}_{\mathrm{Brown}}$ can be calculated by applying a pressure, which has the shape of the intensity profile difference between the two cavity modes. Following the formalisms from Vinet [77], the scaling factor is

$$g_{\Delta(mn)} = S^{(mn)}_{\mathrm{Brown}}/S^{(00)}_{\mathrm{Brown}} = \frac{4}{\pi}\int_0^\infty dp \int_0^\infty dq e^{-(p^2+q^2)}(L_m(p^2) \times L_n(q^2) - L_0(p^2) \times L_0(q^2))^2. \quad \text{(C3)}$$

The numerical values for the first $g_{\Delta(mn)}$ factors can be found in Table V, and the factor relevant for this work is $g_{(00)}/g_{\Delta(01)} = 1.33$. Therefore, from the measured noise in the difference between the HG_{00} and HG_{01} modes, the local (Brownian) noise for any HG_{mn} mode can be calculated.

The correlation coefficient between the coating Brownian thermal noise of an HG_{mn} mode and the HG_{00} mode $\mathrm{Corr}_{(mn)}$ can be calculated as

$$\mathrm{Corr}_{(mn)} = \frac{S^{(00)}_{\mathrm{Brown}} + S^{(01)}_{\mathrm{Brown}} - S^{\Delta(mn)}_{\mathrm{Brown}}}{2\sqrt{S^{(00)}_{\mathrm{Brown}} S^{(mn)}_{\mathrm{Brown}}}} \quad \text{(C4)}$$

TABLE V. Numerical values for $g_{\Delta(mn)}$, the relative PSD of the difference between HG_{mn} and HG_{00} to HG_{00}.

n \ m	0	1	2	3
0	0.000	0.750	0.890	0.949
1	0.750	1.063	1.105	1.118
2	0.890	1.105	1.129	1.133
3	0.949	1.118	1.133	1.134

TABLE VI. Numerical values for the correlation coefficients between Brownian noise of HG_{mn} and HG_{00} mode $Corr_{(mn)}$.

m	0	1	2	3
n				
0	1.000	0.577	0.469	0.412
1	0.577	0.333	0.271	0.238
2	0.469	0.271	0.219	0.194
3	0.412	0.238	0.194	0.171

$$= \frac{1 + g_{(mn)} - g_{\Delta(mn)}}{2\sqrt{g_{(mn)}}}. \tag{C5}$$

The numerical values of the first correlation coefficients $Corr_{(mn)}$ can be found in Table VI.

2. Spatial property of birefringent noise

To investigate the spatial property of the birefringent noise, one needs to compare the noise between the fast and slow modes of two different HG modes, which requires in total four lasers. To avoid the associated complexity, we analyze the birefringent noise with a different approach using only two lasers, where we assume that the noise level of the polarization-independent noise remains constant between different measurements. For these investigations, we stabilize one laser to the fast HG_{00} mode, and the other to the slow HG_{01} mode and record their frequency difference and also the frequency difference of these lasers to two reference lasers (Si2 and the 48-cm ULE cavity). This allows us to determine the noise between the two modes and also the noise of each individual laser from a three-cornered-hat analysis using the two reference lasers. The displacement fluctuations of the two HG modes and their difference can be expressed as

$$d^{(00)\text{fast}}(t) = d^{(00)}_{\text{Brown}}(t) + d_{\text{global}}(t) + d^{(00)}_{\text{birefr}}(t), \tag{C6}$$

$$d^{(01)\text{slow}}(t) = d^{(01)}_{\text{Brown}}(t) + d_{\text{global}}(t) - d^{(01)}_{\text{birefr}}(t), \tag{C7}$$

$$d^{(\Delta)}(t) = d^{(00)}_{\text{Brown}}(t) - d^{(01)}_{\text{Brown}}(t) + d^{(00)}_{\text{birefr}}(t) - d^{(01)}_{\text{birefr}}(t). \tag{C8}$$

The corresponding PSDs, which can be determined experimentally via TCH analysis, are

$$S_d^{(00)\text{fast}} = S^{(00)}_{\text{Brown}} + S_{\text{global}} + S^{(00)}_{\text{birefr}}, \tag{C9}$$

$$S_d^{(01)\text{slow}} = S^{(01)}_{\text{Brown}} + S_{\text{global}} + S^{(01)}_{\text{birefr}}, \tag{C10}$$

$$S_d^{(\Delta)} = S^{(\Delta)}_{\text{Brown}} + S^{(\Delta)}_{\text{birefr}}. \tag{C11}$$

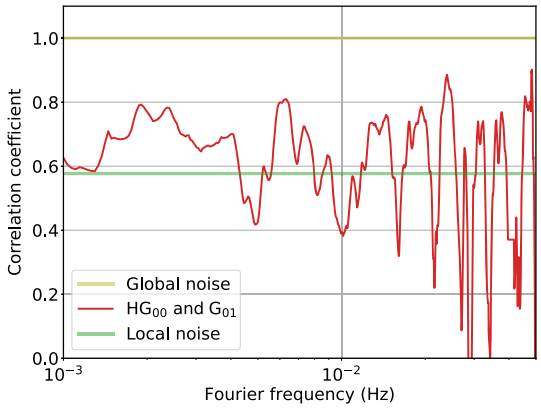

FIG. 12. Correlation coefficient of birefringent noise between the HG_{00} and HG_{01} modes (red). It agrees well with the expectation value for local noise (green) and is significantly different from the expectation value for global noise (yellow).

The PSD $S^{(\Delta)}_{\text{Brown}}$ for the polarization-averaged difference between the HG modes is separately measured using dual-frequency locking to these modes, as well as the PSDs for the polarization-averaged fluctuations

$$S_d^{(00)\text{avg}} = S^{(00)}_{\text{Brown}} + S_{\text{global}}, \tag{C12}$$

$$S_d^{(01)\text{avg}} = S^{(01)}_{\text{Brown}} + S_{\text{global}} \tag{C13}$$

that are obtained from a TCH analysis.

Subtracting these polarization-independent PSDs from Eqs. (C10) and (C11) yields the birefringent noise of the two individual HG modes and their spatially uncorrelated contribution. Based on these values, we calculate the correlation coefficient of the birefringent noise

$$\text{Corr} = \frac{S^{(00)}_{\text{birefr}} + S^{(01)}_{\text{birefr}} - S^{(\Delta)}_{\text{birefr}}}{2 \times \sqrt{S^{(00)}_{\text{birefr}} \times S^{(01)}_{\text{birefr}}}}. \tag{C14}$$

The result 0.59 ± 0.18 agrees with the expected of 0.577 for pure local noise (Table VI) and is well below the global noise (1.00) as shown in Fig. 12, thus indicating the local property of birefringent noise.

3. Power dependence of the photo-birefringent effect

To make sure that the small-signal transfer function can be applied for our estimation of the photo-birefringent noise due to laser power fluctuations, we determine the transfer function by modulating the optical power coupled to the slow axis with different amplitudes ΔP. The average transmitted optical powers in the fast $P_{\text{fast}} = 0.62$ μW and in the slow axis $P_{\text{slow}} = 1.72$ μW are kept constant. The result (Fig. 13) shows that a unique transfer function can be used in our noise estimation.

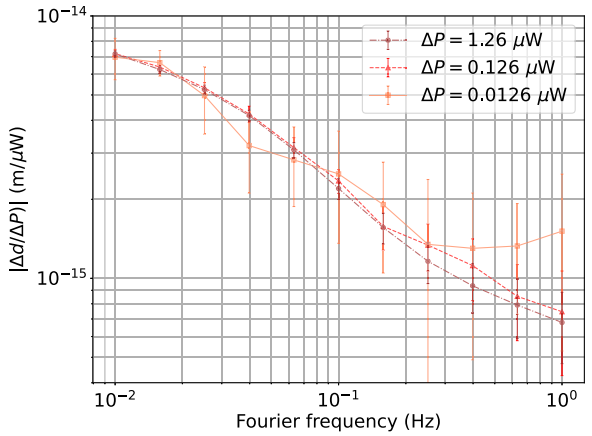

FIG. 13. Small-signal transfer function measured with different modulation amplitude (slow axis) at 0.62 and 1.72 μW mean transmitted power in the fast and slow axes, respectively. The error bars indicate the 95% confidence interval, with contributions from slowly varying electronic offsets, which is estimated by forwarding typical electronic offsets to the slope of PDH error signal.

With constant modulation amplitude of $\Delta P = 0.126\ \mu W$, the transfer function is measured at three different intracavity power levels (Fig. 14). At low Fourier frequencies, the transfer functions depend on the mean transmitted power P_{trans}, which is proportional to the intracavity power: $P_{\mathrm{intra}} \approx 2\mathcal{F}/\pi \times P_{\mathrm{trans}}$, where $\mathcal{F}$ is the finesse and assuming the transmission and loss of the coating are equal. With the finesse of 360 000, we estimate a factor $P_{\mathrm{intra}}/P_{\mathrm{trans}} = 0.229\ \mathrm{W}/\mu\mathrm{W}$. At higher frequencies, the uncertainties are larger and the differences are not significant.

The uncertainty of the transfer function includes statistical uncertainties and contributions from electronic offsets in our measurement. Electronic offsets ΔV arising, e.g., from the rf mixer and rf pickup in the PDH error signal shift the locking frequency away from the cavity resonance by $\Delta\nu = \Delta V/D$, where D is the slope of the PDH error signal that is proportional to the optical power. Hence, modulating the optical power changes the frequency offset $\Delta\nu$ in the PDH lock and adds uncertainty to the measurement. In addition, electronic offset in the control loop for compensation of RAM in combination with the low corner frequency (0.03 Hz) of the RAM loop filter further contributes to the total uncertainty. Using typical values for offsets in these loops, we arrive at the uncertainties shown in Figs. 14 and 3.

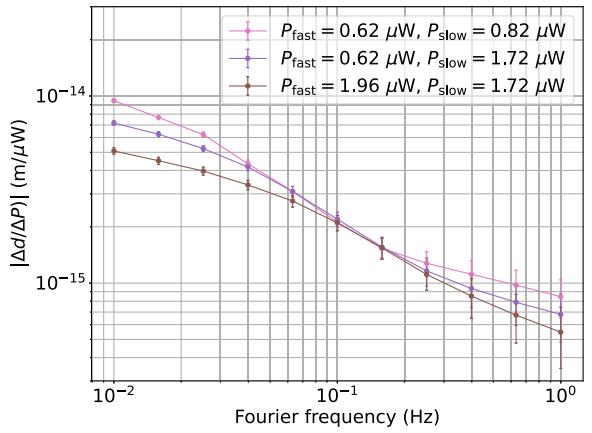

FIG. 14. Small-signal transfer function from optical power modulation in transmission ΔP to optical path length changes Δd for different averaged transmitted power P_{trans}. The error bars have the same meaning as those described in Fig. 13.

APPENDIX D: ESTIMATED INFLUENCE ON THE EINSTEIN TELESCOPE

The ET LF is currently designed to be operated at 10–20 K and 1.5-μm wavelength. One of the candidate test masses is single-crystal silicon mirror substrate with crystalline mirror coatings [4]. The detector has a design beam radius of $w_{\mathrm{ET}} = 9$ cm to reduce the coating Brownian noise well below the quantum noise at an intracavity power level of $P_{\mathrm{ET}} = 18$ kW, and corresponds to a light intensity of $I_{\mathrm{ET}} \approx 71\ \mathrm{W/cm^2}$. The $L_{\mathrm{arm}} = 10$ km arm length of the interferometers further lowers the influence of known coating noise and quantum noise on strain sensitivity to achieve the design value of $h \approx 1 \times 10^{-24}/\mathrm{Hz}$ at $f = 10$ Hz Fourier frequency. This corresponds to the temperature and light intensity that are quite similar to the conditions in our Si6 system. To meet the scientific goal of ET LF [4], the total coating noise PSD must be lower than a quarter of the Brownian thermal noise of the dielectric coating at the operation temperature $S_{\mathrm{Brown}} = 4.5 \times 10^{-40}\,\mathrm{m^2/Hz} \times (f/\mathrm{Hz})^{-1}$, which corresponds to a noise level of $S_{\mathrm{ET}}(10\ \mathrm{Hz}) = 0.25\ S_{\mathrm{Brown}}(10\ \mathrm{Hz}) = 1.2 \times 10^{-41}\ \mathrm{m^2/Hz}$.

From our measurement at 16 K, we observe a birefringent noise level of

$$S_{\mathrm{birefr}}(f) = 2 \times 10^{-34}\ \mathrm{m^2/Hz} \times (f/\mathrm{Hz})^{-1.5} \quad \text{(D1)}$$

with a mode radius of $w_{\mathrm{Si6}} = 290\ \mu$m at $P_{\mathrm{Si6}} = 0.15$ W intracavity power, which corresponds to a light intensity of $I_{\mathrm{Si6}} = 57\ \mathrm{W/cm^2}$. We verify the local property of the birefringent noise which indicates a $1/w^2$ scaling of the noise PSD. Furthermore, we observe an empirical scaling of the birefringent noise by $\sqrt{I}$ [38]. Therefore, we estimate that the birefringent noise for the ET LF as

$$S'_{\mathrm{birefr}}(10\ \mathrm{Hz}) = S_{\mathrm{birefr}}(10\ \mathrm{Hz}) \times \sqrt{\frac{I_{\mathrm{ET}}}{I_{\mathrm{Si6}}}} \times \left(\frac{w_{\mathrm{Si6}}}{w_{\mathrm{ET}}}\right)^2 = 7.3 \times 10^{-41}\ \frac{\mathrm{m^2}}{\mathrm{Hz}}, \quad \text{(D2)}$$

which is 6 times higher than S_{ET} and 1.6 times that of using dielectric coatings. Therefore, if the cancellation of

birefringent noise is impossible in the ET LF, conventional dielectric coatings will outperform the AlGaAs crystalline coating.

When the birefringent noise is canceled, the global excess noise with large correlation length is the dominating noise contribution with a PSD of

$$S_{\text{global}} = 3 \times 10^{-35}\ \text{m}^2/\text{Hz} \times (f/\text{Hz})^{-1} \tag{D3}$$

in Si6 at 16 K. If the coherence length l_{corr} of S_{global} is larger than the beam diameter $2w_{\text{ET}} = 18$ cm, the global excess noise level at 10 Hz would be

$$S'_{\text{global}}(10\ \text{Hz}) = 3 \times 10^{-36}\ \frac{\text{m}^2}{\text{Hz}}. \tag{D4}$$

If the coherence length is on the order of $l_{\text{corr}} = 1$ mm—the lower limit deduced from our measurement—the global excess noise would be reduced to

$$\begin{aligned} S'_{\text{global}}(10\ \text{Hz}) &= S_{\text{global}}(10\ \text{Hz}) \times \left(\frac{l_{\text{corr}}}{2w_{\text{ET}}}\right)^2 \\ &= 9.3 \times 10^{-41}\ \frac{\text{m}^2}{\text{Hz}}, \end{aligned} \tag{D5}$$

which is still 8 times higher than the ET LF design value S_{ET}, and 2.1 times that of using dielectric coatings.

In either case, the current crystalline coating does not meet the requirement of the ET LF.

[1] G. M. Harry, H. Armandula, E. Black, D. R. M. Crooks, G. Cagnoli, J. Hough, P. Murray, S. Reid, S. Rowan, P. Sneddon, M. M. Fejer, R. Route, and S. D. Penn, *Thermal Noise from Optical Coatings in Gravitational Wave Detectors*, Appl. Opt. **45**, 1569 (2006).

[2] S. Hild, M. Abernathy, F. Acernese, P. Amaro-Seoane, N. Andersson, K. Arun, F. Barone, B. Barr, M. Barsuglia, M. Beker, N. Beveridge, S. Birindelli, S. Bose, L. Bosi, S. Braccini, C. Bradaschia, T. Bulik, E. Calloni, G. Cella, E. C. Mottin *et al.*, *Sensitivity Studies for Third-Generation Gravitational Wave Observatories*, Classical Quantum Gravity **28**, 094013 (2011).

[3] R. X. Adhikari, K. Arai, A. F. Brooks, C. Wipf, O. Aguiar, P. Altin, B. Barr, L. Barsotti, R. Bassiri, A. Bell, G. Billingsley, R. Birney, D. Blair, E. Bonilla, J. Briggs, D. D. Brown, R. Byer, H. Cao, M. Constancio, S. Cooper *et al.*, *A Cryogenic Silicon Interferometer for Gravitational-Wave Detection*, Classical Quantum Gravity **37**, 165003 (2020).

[4] ET Editorial Team, *Design Report Update 2020 for the Einstein Telescope*, 2020, https://www.et-gw.eu/index.php/relevant-et-documents.

[5] T. Kessler, C. Hagemann, C. Grebing, T. Legero, U. Sterr, F. Riehle, M. J. Martin, L. Chen, and J. Ye, *A Sub-40-mHz-Linewidth Laser Based on a Silicon Single-Crystal Optical Cavity*, Nat. Photonics **6**, 687 (2012).

[6] S. Häfner, S. Falke, C. Grebing, S. Vogt, T. Legero, M. Merimaa, C. Lisdat, and U. Sterr, 8×10^{-17} *Fractional Laser Frequency Instability with a Long Room-Temperature Cavity*, Opt. Lett. **40**, 2112 (2015).

[7] D. G. Matei, T. Legero, S. Häfner, C. Grebing, R. Weyrich, W. Zhang, L. Sonderhouse, J. M. Robinson, J. Ye, F. Riehle, and U. Sterr, 1.5 μm *Lasers with Sub-10 mHz Linewidth*, Phys. Rev. Lett. **118**, 263202 (2017).

[8] W. Zhang, J. M. Robinson, L. Sonderhouse, E. Oelker, C. Benko, J. L. Hall, T. Legero, D. G. Matei, F. Riehle, U. Sterr, and J. Ye, *Ultrastable Silicon Cavity in a Continuously Operating Closed-Cycle Cryostat at 4 K*, Phys. Rev. Lett. **119**, 243601 (2017).

[9] E. Oelker, R. B. Hutson, C. J. Kennedy, L. Sonderhouse, T. Bothwell, A. Goban, D. Kedar, C. Sanner, J. M. Robinson, G. E. Marti, D. G. Matei, T. Legero, M. Giunta, R. Holzwarth, F. Riehle, U. Sterr, and J. Ye, *Demonstration of* 4.8×10^{-17} *Stability at 1 s for Two Independent Optical Clocks*, Nat. Photonics **13**, 714 (2019).

[10] R. Lange, A. A. Peshkov, N. Huntemann, C. Tamm, A. Surzhykov, and E. Peik, *Lifetime of the* $^2F_{7/2}$ *Level in* Yb^+ *for Spontaneous Emission of Electric Octupole Radiation*, Phys. Rev. Lett. **127**, 213001 (2021).

[11] T. Bothwell, C. J. Kennedy, A. Aeppli, D. Kedar, J. M. Robinson, E. Oelker, A. Staron, and J. Ye, *Resolving the Gravitational Redshift across a Millimetre-Scale Atomic Sample*, Nature (London) **602**, 420 (2022).

[12] P. Delva, J. Lodewyck, S. Bilicki, E. Bookjans, G. Vallet, R. L. Targat, P.-E. Pottie, C. Guerlin, F. Meynadier, C. L. Poncin-Lafitte, O. Lopez, A. Amy-Klein, W.-K. Lee, N. Quintin, C. Lisdat, A. Al-Masoudi, S. Dörscher, C. Grebing, G. Grosche, A. Kuhl *et al.*, *Test of Special Relativity Using a Fiber Network of Optical Clocks*, Phys. Rev. Lett. **118** (2017).

[13] C. J. Kennedy, E. Oelker, J. M. Robinson, T. Bothwell, D. Kedar, W. R. Milner, G. E. Marti, A. Derevianko, and J. Ye, *Precision Metrology Meets Cosmology: Improved Constraints on Ultralight Dark Matter from Atom-Cavity Frequency Comparisons*, Phys. Rev. Lett. **125**, 201302 (2020).

[14] R. Lange, N. Huntemann, J. M. Rahm, C. Sanner, H. Shao, B. Lipphardt, C. Tamm, S. Weyers, and E. Peik, *Improved Limits for Violations of Local Position Invariance from Atomic Clock Comparisons*, Phys. Rev. Lett. **126**, 011102 (2021).

[15] V. Debierre, C. Keitel, and Z. Harman, *Fifth-Force Search with the Bound-Electron g Factor*, Phys. Lett. B **807**, 135527 (2020).

[16] F. Riehle, *Towards a Redefinition of the Second Based on Optical Atomic Clocks*, C. R. Phys. **16**, 506 (2015).

[17] J. Lodewyck, *On a Definition of the SI Second with a Set of Optical Clock Transitions*, Metrologia **56**, 055009 (2019).

[18] S. C. Tait, J. Steinlechner, M. M. Kinley-Hanlon, P. G. Murray, J. Hough, G. McGhee, F. Pein, S. Rowan, R. Schnabel, C. Smith, L. Terkowski, and I. W. Martin, *Demonstration of the Multimaterial Coating Concept to Reduce Thermal Noise in Gravitational-Wave Detectors*, Phys. Rev. Lett. **125**, 011102 (2020).

[19] H.-W. Pan, L.-C. Kuo, L.-A. Chang, S. Chao, I. W. Martin, J. Steinlechner, and M. Fletcher, *Silicon Nitride and Silica Quarter-Wave Stacks for Low-Thermal-Noise Mirror Coatings*, Phys. Rev. D **98**, 102001 (2018).

[20] J. Steinlechner, I. W. Martin, A. S. Bell, J. Hough, M. Fletcher, P. G. Murray, R. Robie, S. Rowan, and R. Schnabel, *Silicon-Based Optical Mirror Coatings for Ultrahigh Precision Metrology and Sensing*, Phys. Rev. Lett. **120**, 263602 (2018).

[21] G. Vajente, R. Birney, A. Ananyeva, S. Angelova, R. Asselin, B. Baloukas, R. Bassiri, G. Billingsley, M. M. Fejer, D. Gibson, L. J. Godbout, E. Gustafson, A. Heptonstall, J. Hough, S. MacFoy, A. Markosyan, I. W. Martin, L. Martinu, P. G. Murray, S. Penn *et al.*, *Effect of Elevated Substrate Temperature Deposition on the Mechanical Losses in Tantala Thin Film Coatings*, Classical Quantum Gravity **35**, 075001 (2018).

[22] M. Magnozzi, S. Terreni, L. Anghinolfi, S. Uttiya, M. Carnasciali, G. Gemme, M. Neri, M. Principe, I. Pinto, L.-C. Kuo, S. Chao, and M. Canepa, *Optical Properties of Amorphous* SiO_2-TiO_2 *Multi-Nanolayered Coatings for 1064-nm Mirror Technology*, Opt. Mater. **75**, 94 (2018).

[23] J. M. Robinson, E. Oelker, W. R. Milner, D. Kedar, W. Zhang, T. Legero, D. G. Matei, S. Häfner, F. Riehle, U. Sterr, and J. Ye, *Thermal Noise and Mechanical Loss of* SiO_2/Ta_2O_5 *Optical Coatings at Cryogenic Temperatures*, Opt. Lett. **46**, 592 (2021).

[24] H. J. Kimble, B. L. Lev, and J. Ye, *Optical Interferometers with Reduced Sensitivity to Thermal Noise*, Phys. Rev. Lett. **101**, 260602 (2008).

[25] J. Dickmann and S. Kroker, *Highly Reflective Low-Noise Etalon-Based Meta-Mirror*, Phys. Rev. D **98**, 082003 (2018).

[26] H. B. Callen and T. A. Welton, *Irreversibility and Generalized Noise*, Phys. Rev. **83**, 34 (1951).

[27] R. Kubo, *The Fluctuation-Dissipation Theorem*, Rep. Prog. Phys. **29**, 255 (1966).

[28] Y. Levin, *Internal Thermal Noise in the LIGO Test Masses: A Direct Approach*, Phys. Rev. D **57**, 659 (1998).

[29] J. Steinlechner, *Development of Mirror Coatings for Gravitational-Wave Detectors*, Phil. Trans. R. Soc. A **376**, 20170282 (2018).

[30] G. M. Harry, M. R. Abernathy, A. E. Becerra-Toledo, H. Armandula, E. Black, K. Dooley, M. Eichenfield, C. Nwabugwu, A. Villar, D. R. M. Crooks, G. Cagnoli, J. Hough, C. R. How, I. MacLaren, P. Murray, S. Reid, S. Rowan, P. H. Sneddon, M. M. Fejer, R. Route *et al.*, *Titania-Doped Tantala/Silica Coatings for Gravitational-Wave Detection*, Classical Quantum Gravity **24**, 405 (2006).

[31] M. Granata, A. Amato, G. Cagnoli, M. Coulon, J. Degallaix, D. Forest, L. Mereni, C. Michel, L. Pinard, B. Sassolas, and J. Teillon, *Progress in the Measurement and Reduction of Thermal Noise in Optical Coatings for Gravitational-Wave Detectors*, Appl. Opt. **59**, A229 (2020).

[32] K. A. Topp and D. G. Cahill, *Elastic Properties of Several Amorphous Solids and Disordered Crystals below 100 K*, Z. Phys. B **101**, 235 (1996).

[33] G. D. Cole, *Cavity Optomechanics with Low-Noise Crystalline Mirrors*, Proc. SPIE Int. Soc. Opt. Eng. **8458**, 845807 (2012).

[34] S. D. Penn, M. M. Kinley-Hanlon, I. A. O. MacMillan, P. Heu, D. Follman, C. Deutsch, G. D. Cole, and G. M. Harry, *Mechanical Ringdown Studies of Large-Area Substrate-Transferred* GaAs/AlGaAs *Crystalline Coatings*, J. Opt. Soc. Am. B **36**, C15 (2019).

[35] K. Yamamoto, S. Miyoki, T. Uchiyama, H. Ishitsuka, M. Ohashi, K. Kuroda, T. Tomaru, N. Sato, T. Suzuki, T. Haruyama, A. Yamamoto, T. Shintomi, K. Numata, K. Waseda, K. Ito, and K. Watanabe, *Measurement of the Mechanical Loss of a Cooled Reflective Coating for Gravitational Wave Detection*, Phys. Rev. D **74**, 022002 (2006).

[36] T. Legero, D. G. Matei, R. Weyrich, S. Häfner, Fritz Riehle, L. Sonderhouse, J. M. Robinson, E. Oelker, W. Zhang, J. Ye, P. Heu, D. Follman, C. Deutsch, G. Cole, and U. Sterr, *Towards a Cryogenic Silicon Resonator with Low Thermal Noise Crystalline Mirrors*, in *Proceedings of the European Frequency and Time Forum (EFTF), Torino, Italy*, 2018, p. 75, https://www.eftf.org/fileadmin/documents/eftf/documents/Proceedings/proceedingsEFTF2018.pdf.

[37] G. D. Cole, W. Zhang, M. J. Martin, J. Ye, and M. Aspelmeyer, *Tenfold Reduction of Brownian Noise in Optical Interferometry*, Nat. Photonics **7**, 644 (2013).

[38] D. Kedar, J. Yu, E. Oelker, A. Staron, W. R. Milner, J. M. Robinson, T. Legero, F. Riehle, U. Sterr, and J. Ye, *Frequency Stability of Cryogenic Silicon Cavities with Semiconductor Crystalline Coatings*, Optica **10**, 464 (2023).

[39] G. Winkler, L. W. Perner, G.-W. Truong, G. Zhao, D. Bachmann, A. S. Mayer, J. Fellinger, D. Follman, P. Heu, C. Deutsch, D. M. Bailey, H. Peelaers, S. Puchegger, A. J. Fleisher, G. D. Cole, and O. H. Heckl, *Mid-Infrared Interference Coatings with Excess Optical Loss below 10 ppm*, Optica **8**, 686 (2021).

[40] J. M. Robinson, E. Oelker, W. R. Milner, W. Zhang, T. Legero, D. G. Matei, F. Riehle, U. Sterr, and J. Ye, *Crystalline Optical Cavity at 4 K with Thermal Noise Limited Instability and Ultralow Drift*, Optica **6**, 240 (2019).

[41] T. Kessler, T. Legero, and U. Sterr, *Thermal Noise in Optical Cavities Revisited*, J. Opt. Soc. Am. B **29**, 178 (2012).

[42] V. B. Braginsky, M. L. Gorodetsky, and S. P. Vyatchanin, *Thermodynamical Fluctuations and Photo-Thermal Shot Noise in Gravitational Wave Antennae*, Phys. Lett. A **264**, 1 (1999).

[43] D. I. Babic and S. W. Corzine, *Analytic Expressions for the Reflection Delay, Penetration Depth, and Absorptance of Quarter-Wave Dielectric Mirrors*, IEEE J. Quantum Electron. **28**, 514 (1992).

[44] F. Brandi, F. Della Valle, A. De Riva, P. Micossi, F. Perrone, C. Rizzo, G. Ruoso, and G. Zavattini, *Measurement of the Phase Anisotropy of Very High Reflectivity Interferential Mirrors*, Appl. Phys. B **65**, 351 (1997).

[45] E. D. Black, *An Introduction to Pound-Drever-Hall Laser Frequency Stabilization*, Am. J. Phys. **69**, 79 (2001).

[46] S. Gras, H. Yu, W. Yam, D. Martynov, and M. Evans, *Audio-Band Coating Thermal Noise Measurement for Advanced LIGO with a Multi-Mode Optical Resonator*, Phys. Rev. D **95**, 022001 (2017).

[47] A. Farsi, M. Siciliani de Cumis, F. Marino, and F. Marin, *Photothermal and Thermo-Refractive Effects in High*

Reflectivity Mirrors at Room and Cryogenic Temperature, J. Appl. Phys. **111**, 043101 (2012).

[48] T. Chalermsongsak, E. D. Hall, G. D. Cole, D. Follman, F. Seifert, K. Arai, E. K. Gustafson, J. R. Smith, M. Aspelmeyer, and R. X. Adhikari, *Coherent Cancellation of Photothermal Noise in* $GaAs/Al_{0.92}Ga_{0.08}As$ *Bragg Mirrors*, Metrologia **53**, 860 (2016).

[49] S. Herbers, *Transportable Ultra-Stable Laser System with an Instability Down to* 10^{-16}, Ph.D. thesis, Gottfried Wilhelm Leibniz Universität, 2021.

[50] S. Namba, *Electro-Optical Effect of Zincblende*, J. Opt. Soc. Am. **51**, 76 (1961).

[51] R. Twu and Y. Chu, *Measurements of Photorefractive Birefringence on the Different Propagation Directions in Electro-Optic Crystals*, Measurement **121**, 1 (2018).

[52] P. Minzioni, I. Cristiani, and V. Degiorgio, *Strongly Sublinear Growth of the Photorefractive Effect for Increasing Pump Intensities in Doped Lithium-Niobate Crystals*, J. Appl. Phys. **101**, 116105 (2007).

[53] F. Agulló-López, G. F. Calvo, and M. Carrascosa, *Fundamentals of Photorefractive Phenomena*, in *Photorefractive Materials and Their Applications 1*, edited by P. Günter and J. P. Huignard, Springer Series in Optical Sciences Vol. 113 (Springer, New York, 2006), 10.1007/0-387-25192-8_3.

[54] E. Estacio, M. Bailon, A. Somintac, R. Sarmiento, and A. Salvador, *Observation of High Junction Electric Fields in Modulation-Doped* GaAs/AlGaAs *Heterostructures by Room Temperature Photoreflectance Spectroscopy*, J. Appl. Phys. **91**, 3717 (2002).

[55] S. Gras and M. Evans, *Direct Measurement of Coating Thermal Noise in Optical Resonators*, Phys. Rev. D **98**, 122001 (2018).

[56] J. G. Hartnett, D. Mouneyrac, J.-M. Le Floch, J. Krupka, M. E. Tobar, and D. Cros, *Observation of Persistent Photoconductivity in Bulk Gallium Arsenide and Gallium Phosphide Samples at Cryogenic Temperatures Using the Whispering Gallery Mode Method*, J. Appl. Phys. **104**, 113714 (2008).

[57] V. I. Borisov, V. A. Sablikov, I. V. Borisova, and A. I. Chmil, *Charging of Deep-Level Centers and Negative Persistent Photoconductivity in Modulation-Doped* AlGaAs/GaAs *Heterostructures*, Semiconductors **33**, 60 (1999).

[58] J. Steinlechner and I. W. Martin, *How Can Amorphous Silicon Improve Current Gravitational-Wave Detectors*, Phys. Rev. D **103**, 042001 (2021).

[59] C. Hagemann, *Ultra-Stable Laser Based on a Cryogenic Single-Crystal Silicon Cavity*, Ph. D. thesis, Gottfried Wilhelm Leibniz Universität Hannover, 2013.

[60] W. Zhang, M. J. Martin, C. Benko, J. L. Hall, J. Ye, C. Hagemann, T. Legero, U. Sterr, F. Riehle, G. D. Cole, and M. Aspelmeyer, *Reduction of Residual Amplitude Modulation to* 1×10^{-6} *for Frequency-Modulation and Laser Stabilization*, Opt. Lett. **39**, 1980 (2014).

[61] L.-S. Ma, P. Jungner, J. Ye, and J. L. Hall, *Delivering the Same Optical Frequency at Two Places: Accurate Cancellation of Phase Noise Introduced by Optical Fiber or Other Time-Varying Path*, Opt. Lett. **19**, 1777 (1994).

[62] J. Kawohl, *Entwicklung eines digitalen Reglersystems zur aktiven Schwingungsisolation optischer Resonatoren*, Master's thesis, Technische Universität Braunschweig, 2021.

[63] A. Premoli and P. Tavella, *A Revisited Three-Cornered Hat Method for Estimating Frequency Standard Instability*, IEEE Trans. Instrum. Meas. **42**, 7 (1993).

[64] M. Evans, S. Ballmer, M. Fejer, P. Fritschel, G. Harry, and G. Ogin, *Thermo-Optic Noise in Coated Mirrors for High-Precision Optical Measurements*, Phys. Rev. D **78**, 102003 (2008).

[65] W. A. Brantley, *Calculated Elastic Constants for Stress Problems Associated with Semiconductor Devices*, J. Appl. Phys. **44**, 534 (1973).

[66] H. J. McSkimin, *Measurement of Elastic Constants at Low Temperatures by Means of Ultrasonic Waves–Data for Silicon and Germanium Single Crystals, and for Fused Silica*, J. Appl. Phys. **24**, 988 (1953).

[67] C. J. Glassbrenner and G. A. Slack, *Thermal Conductivity of Silicon and Germanium from* 3 °K *to the Melting Point*, Phys. Rev. **134**, A1058 (1964).

[68] P. Flubacher, A. J. Leadbetter, and J. A. Morrison, *The Heat Capacity of Pure Silicon and Germanium and Properties of Their Vibrational Frequency Spectra*, Philos. Mag. **4**, 273 (1959).

[69] R. Nawrodt, A. Zimmer, T. Koettig, D. H. Christian Schwarz, M. Hudl, R. Neubert, M. Thürk, S. Nietzsche, W. Vodel, P. Seidel, and A. Tünnermann, *High Mechanical Q-Factor Measurements on Silicon Bulk Samples*, J. Phys. Conf. Ser. **122**, 012008 (2008).

[70] *Properties of Aluminium Gallium Arsenide*, EMIS Datareviews Series No. 7, edited by S. Adachi (The Institution of Electrical Engineers, London, 1993).

[71] D. W. Jenkins, *Optical Constants of* $Al_xGa_{1-x}As$, J. Appl. Phys. **68**, 1848 (1990).

[72] M. A. Afromowitz, *Thermal Conductivity of* $Ga_{1-x}Al_xAs$ *Alloys*, J. Appl. Phys. **44**, 1292 (1973).

[73] J. S. Blakemore, *Semiconducting and Other Major Properties of Gallium Arsenide*, J. Appl. Phys. **53**, R123 (1982).

[74] K. P. Birch and M. J. Downs, *Correction to the Updated Edlén Equation for the Refractive Index of Air*, Metrologica **31**, 315 (1994).

[75] R. W. P. Drever, J. L. Hall, F. V. Kowalski, J. Hough, G. M. Ford, A. J. Munley, and H. Ward, *Laser Phase and Frequency Stabilization Using an Optical Resonator*, Appl. Phys. B **31**, 97 (1983).

[76] N. C. Wong and J. L. Hall, *Servo Control of Amplitude Modulation in Frequency-Modulation Spectroscopy: Demonstration of Shot-Noise-Limited Detection*, J. Opt. Soc. Am. B **2**, 1527 (1985).

[77] J.-Y. Vinet, *Thermal Noise in Advanced Gravitational Wave Interferometric Antennas: A Comparison between Arbitrary Order Hermite and Laguerre Gaussian Modes*, Phys. Rev. D **82**, 042003 (2010).